

Nonlinearly driven transverse synchronization in coupled chaotic systems

Massimo Cencini ^(a) and Alessandro Torcini ^(b)

^(a) ISC-CNR Via dei Taurini 19, I-00185 Roma, Italy and SM C-INFM, Dip.
Fisica, Università di Roma "La Sapienza", p.zza Aldo Moro 2, I-00185 Roma,
Italy

^(b) ISC-CNR, Sezione Territoriale di Firenze, and Istituto Nazionale di Ottica
Applicata, L.go E. Fermi, 6 - I-50125 Firenze, Italy

Abstract

Synchronization transitions are investigated in coupled chaotic maps. Depending on the relative weight of linear versus nonlinear instability mechanisms associated to the single map two different scenarios for the transition may occur. When only two maps are considered we always find that the critical coupling μ_1 for chaotic synchronization can be predicted within a linear analysis by the vanishing of the transverse Lyapunov exponent λ_T . However, major differences between transitions driven by linear or nonlinear mechanisms are revealed by the dynamics of the transient toward the synchronized state. As a representative example of extended systems a one dimensional lattice of chaotic maps with power-law coupling is considered. In this high dimensional model finite amplitude instabilities may have a dramatic effect on the transition. For strong nonlinearities an exponential divergence of the synchronization times with the chain length can be observed above μ_1 , notwithstanding the transverse dynamics is stable against infinitesimal perturbations at any instant. Therefore, the transition takes place at a coupling μ_{n1} definitely larger than μ_1 and its origin is intrinsically nonlinear. The linearly driven transitions are continuous and can be described in terms of mean field results for non-equilibrium phase transitions with long range interactions. While the transitions dominated by nonlinear mechanisms appear to be discontinuous.

Key words: synchronization; coupled chaotic systems; linear and nonlinear instabilities; coupled map lattices

PACS: 05.45.-a, 05.45.Xt, 05.45.Ra

1 Introduction

Synchronization is a phenomenon observed in many different contexts, ranging from epidemics spreading [1] to neuro-sciences [2]. The analysis of simple models pursued in the last two decades has clarified several aspects of synchronization (for a comprehensive review on the subject see Ref. [3]).

Particularly interesting both from a theoretical and an applied point of view is synchronization of chaotic systems. This is a phenomenon known since many years [4] with important applications, e.g., in secure communications of digital signals, laser dynamics etc. A simple but not trivial framework to study chaotic synchronization is represented by discrete-time dynamical systems. Within this context, the essence of the phenomenon can be captured already by considering two coupled identical maps:

$$\begin{aligned}x^{t+1} &= (1 - \epsilon)f(x^t) + \epsilon f(y^t) \\ y^{t+1} &= \epsilon f(x^t) + (1 - \epsilon)f(y^t); \end{aligned} \quad (1)$$

where $f(x)$ is a chaotic map of the unit interval and ϵ the coupling constant. For coupling larger than a critical value ϵ_1 a transition from a desynchronized state to a completely synchronized one along a chaotic orbit x^t is observed, i.e. $x^t = y^t$ for $\epsilon > \epsilon_1$. The coupling ϵ_1 can be predicted within a linear analysis as the value of ϵ for which the Transverse Lyapunov Exponent (TLE) λ_T , ruling the instabilities transversal to the line $x = y$, vanishes. For model (1) $\lambda_T = \ln(1 - 2\epsilon) + \lambda_0$ [3], and consequently

$$\epsilon_1 = \frac{1 - e^{\lambda_0}}{2}; \quad (2)$$

being λ_0 the Lyapunov Exponent (LE) of the single (uncoupled) map.

While in low dimensional systems the basic mechanisms ruling synchronization, in the absence of strong nonlinear effects, have been well established since long time [3,5,6], the studies devoted to synchronization in extended systems are still limited to few specific examples [7,8,9,10]. In the latter case, two main frameworks have been considered.

On one hand, the investigation of mutual synchronization between two replicas of a spatially extended system has been pursued for systems coupled either via local interaction [9] or via spatio-temporal noise [8]. In both cases, when the amplitude of the coupling (noise) overcomes a certain threshold, synchronization is observed: after a transient, the two systems follow the same spatio-temporal chaotic (stochastic) orbit.

On the other hand, another commonly observed situation corresponds to self

synchronization of elements belonging to the same system. This occurs for instance in large collections of coupled elements such as populations of neurons [11], Josephson junctions [12] or cardiac pacemaker cells [13]. In these systems the interaction among the elements can range from nearest neighbors to globally coupled. Therefore, a model able to encompass both these limiting cases is certainly of interest. A good candidate is represented by the following coupled map lattice with power-law interactions [14,15,10]

$$x_i^{t+1} = (1 - \epsilon) f(x_i^t) + \frac{\epsilon}{L^0} \sum_{k=1}^{L^0} \frac{f(x_{i-k}^t) + f(x_{i+k}^t)}{k}; \quad (3)$$

which reduces to globally coupled maps (GCM's) [16] for $\epsilon = 0$, and to standard coupled map lattices (CML's) with nearest neighbor coupling [17] in the limit $\epsilon \rightarrow 1$. In equation (3), t and i are the discrete temporal and spatial indexes, L is the lattice size ($i = 1; \dots; L$), x_i^t the state variable, $\epsilon \in [0 : 1]$ measures the strength of the coupling and its power-law decay. Since the sum extends up to $L^0 = (L - 1)/2$ the model is well defined only for odd L -values, and $L^0 = \lfloor (L - 1)/2 \rfloor$ is a normalization factor. Periodic boundary conditions are assumed.

The synchronization between replicas of the same spatial system has been the subject of a more systematic study than self-synchronization and is now rather well understood [8,18,9,19,20]. Two different mechanisms of mutual synchronization have been identified according to the predominance of linear versus nonlinear effects. Nonlinearly dominated transitions are observed when the local dynamics is ruled by a discontinuous (e.g. the Bernoulli map) or "almost discontinuous" maps (e.g. maps possessing very high values of the first derivatives). In these cases a linear analysis is no more sufficient to fully characterize the transition, because the instabilities associated with finite amplitude perturbations may desynchronize the system. In both cases the transition to the synchronized state is typically of the second order. However, depending on the linear or non-linear nature of the prevailing mechanism two different universality classes characterize the transition itself. For continuous maps (e.g. logistic maps) critical exponents associated with the Multiplicative Noise (MN) universality class are usually found [21], while for (almost) discontinuous maps the transition belongs to the Directed Percolation (DP) class [22].

The aim of the present work is to clarify the effect of strong nonlinearities in the synchronization phenomenon, in particular in the case of self-synchronization.

As a first point, we show that strong nonlinearities may induce nontrivial effects also in low dimensional systems such as two coupled maps. In particular, we find that even though the critical coupling ϵ_1 can be always predicted within the linear framework, the transient dynamics preceding the synchronization can be strongly affected by finite scale instabilities. To properly characterize

the latter we introduce a new indicator, the Finite Size Transverse Lyapunov Exponent (FSTLE), which generalizes the concept of Finite Size Lyapunov Exponent (FSLE) [23,24,25] to the transverse dynamics. The FSTLE extends the definition of TLE to finite perturbation and is therefore able to discern linearly from nonlinearly dominated transitions. Depending on the behavior of the FSTLE at finite amplitudes two different class of maps are singled out: class I maps characterized by a decreasing FSTLE at any finite scale, and class II maps that present a peak in the FSTLE for some finite amplitude value. Moreover, in the proximity of the transition the shape of the probability density function (PDF), $P(\tau)$, of the synchronization times depends on the dynamics at finite scales and on the multifractal properties of the map. For class I maps two cases can be identified. For maps, such as the symmetric tent map and the logistic map at the crisis, which are characterized by the vanishing of fluctuations of the finite time LE at long times, the PDF exhibits a fast falloff at large τ 's. In particular, for the symmetrical tent map we provide an analytical expression for $P(\tau)$. For maps, such as the skew tent map, exhibiting modulational intermittency [3] (which is related to the persistence of fluctuations of the finite time LE also in the long time limit), $P(\tau)$ becomes an inverse Gaussian distribution [26] originating by the diffusive motion of the (logarithm of the) perturbation in transverse space. For class II maps the PDF's display an exponential tail at long times which, differently from the previous case, is due to nonlinear effects.

As far as spatially extended systems are concerned, Anteneodo et al. [10] have performed a linear stability analysis of model (3) obtaining analytically the critical coupling κ_1 for the transition. This prediction works perfectly for class I maps, as found for the coupled logistic maps [10]. However, as shown in the present paper, linear analysis may fail in class II maps. In particular, for large system sizes ($L \gg 1$) an exponential divergence of the synchronization times with L can be observed even for negative TLE, as a result in the limit $L \rightarrow \infty$ the transition takes place at a critical coupling $\kappa_{n1} > \kappa_1$. Finite scale instabilities are the key elements for observing this nonlinear synchronization transition. Similarly to the case of diffusively coupled map lattices it is possible to link the synchronization transition of CML with power law coupling with non-equilibrium phase transitions. Indeed as shown in Ref. [21] synchronization of replicas of CML with short range coupling belong either to the MN or to the DP universality classes. Here we shall discuss the connection of self synchronization of model (3) with long range spreading processes [22,27].

The material is organized as follows. Sect. 2 is devoted to synchronization of two coupled maps. In Sect. 3 coupled maps with power law coupling are examined. Finally in Sec. 4 we briefly summarize the reported results.

2 Synchronization of two coupled identical maps

To analyze the synchronization of two coupled maps (1) it is useful to introduce the following variables:

$$u^t = \frac{x^t + y^t}{2} \quad w^t = \frac{x^t - y^t}{2};$$

in terms of which Eq. (1) can be rewritten as

$$\begin{aligned} u^{t+1} &= \frac{1}{2} [f(u^t + w^t) + f(u^t - w^t)] \\ w^{t+1} &= \frac{1}{2} [\mu^h f(u^t + w^t) - \mu^i f(u^t - w^t)]; \end{aligned} \quad (4)$$

It is easily checked that the synchronized solution (corresponding to $w^t = 0$ and $u^t = f(u^t)$) is an admissible solution of (4) for any value of the coupling μ . The stability of such a solution can be studied by considering the linear dynamics of an infinitesimal perturbation w^t of the synchronized state. This evolves according to the linearized equation:

$$w^{t+1} = (1 - 2\mu) f^0(u^t) w^t; \quad (5)$$

where $f^0 = df/dx$. Clearly the stability of the state $w^t = 0$ is controlled by the sign of the transverse (or conditional) Lyapunov exponent

$$\lambda_T = \ln(1 - 2\mu) + \lambda_0; \quad (6)$$

where λ_0 is the Lyapunov exponent of the single map $f(x)$. Therefore, by requiring $\lambda_T = 0$ one obtains the critical coupling μ_1 (2) above which the synchronized state is linearly stable. Notice that for $\mu = \mu_1$, λ_T coincides with the second Lyapunov exponent λ_2 of the coupled system (1).

The synchronization transition has been mainly studied for continuous maps, here denoted as class I maps, in particular for the logistic map $f(x) = 4x(1-x)$ at the crisis [5] and the skew tent map [6]

$$f(x) = \begin{cases} x & \text{if } 0 \leq x \leq a \\ (1-x)/(1-a) & \text{if } a < x \leq 1 \end{cases}; \quad (7)$$

It should be noticed that inside this class of maps one has to distinguish between two situations according to the behavior of the fluctuations of the finite time Lyapunov exponents in the long time limit. The vanishing of such fluctuations is observed for the symmetric tent map and the logistic one at the

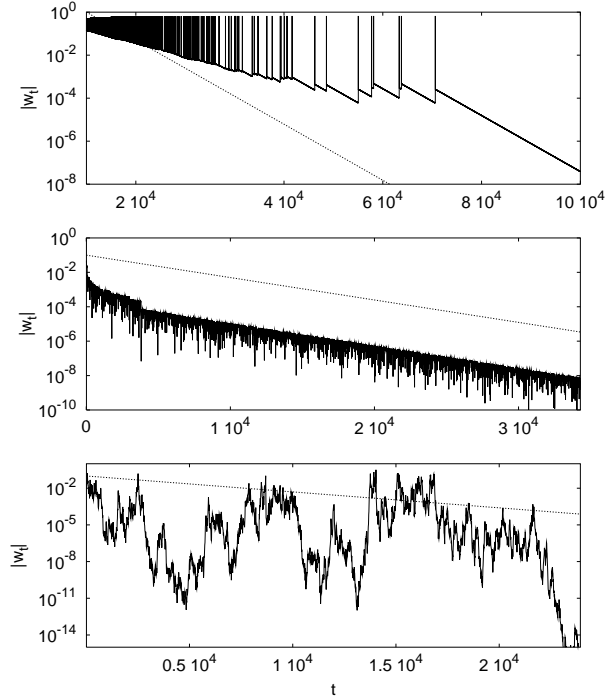


Fig. 1. Typical evolution of $|w_t| = |x_t - y_t|$ starting from random initial conditions. From top: Bernoulli map with $r = 1.5$, logistic map at the crisis and the skew tent map with $a = 2/3$. For all maps, the coupling has been chosen in order to ensure $\tau = 3 \cdot 10^4$. The dashed straight lines display the $e^{-t/\tau}$ decay.

crisis, while their persistence characterizes the skew tent map that represents the generic case [3].

Recent studies however pointed out that discontinuous or "almost" discontinuous maps (i.e. maps with $f^{(0)} \neq 1$ in some point of the definition interval), here termed class II maps, may give rise to non trivial interesting phenomena. For instance, the synchronization transition for two replicas of class II CMLs is not driven, as usual, by infinitesimal perturbations, but by the instability (spreading) of finite amplitude perturbations [8,9]. This nonlinear synchronization is linked to the so-called stable chaos [28]: a phenomenon characterized by information propagation even in the absence of chaos [29,25]. Moreover, as we shall show in the following also the self synchronization of a single CML can be strongly affected by nonlinearities.

Representative examples of class II maps are the generalized Bernoulli map $f(x) = rx \bmod 1$ that is discontinuous and its continuous version

$$f(x) = \begin{cases} a_1 x & 0 < x < x_1 \\ m(x - x_2) & x_1 < x < x_2 \\ a_1(x - x_2) & x_2 < x < 1 \end{cases} \quad (8)$$

with $a_1 = 1=x_1$, $x_{1,2} = 1=a$, $m = 1=2$). As already mentioned, the peculiarity of such maps is that they are not only unstable with respect to infinitesimal perturbations but also to finite ones (for (8) this is true for sufficiently small values).

The main differences between synchronization transitions ruled by linear mechanisms with respect to those driven by finite amplitude instabilities can be captured already by considering the evolution of jw^t . The typical behavior of this quantity for $a > 1$ is reported in Fig. 1 for the Bernoulli, the logistic and the skew tent map. For the logistic map, apart from (short time) fluctuations due to the multiplier variations, an average linear decrease of $\ln jw^t$ with slope given by λ_T is observed. For the Bernoulli map, despite the TLE is negative and does not fluctuate in time, jw^t exhibits instantaneous jumps to 0 (1) values. These jumps, which are due to finite amplitude instabilities, are more probable for large jw^t amplitudes. Completely analogous behaviors have been found for the map (8), where the multipliers do fluctuate.

As shown in Fig. 1 for the skew tent map with $a > 1=2$, jw^t displays an intermittent evolution during the transient preceding the synchronization, that is reflected in a disusive motion of $\ln jw^t$. As a consequence long transients are observed close to the transition. This phenomenon, known as Modulation Intermittency [3] is induced by fluctuations of the finite time TLE that do not average out in the long time limit and as a consequence can be explained by linear analysis.

For the sake of completeness, we mention that long synchronization transients have been reported also for nonlinearly coupled expanding maps [7]. In this model resurgences of jw^t during the transient are due to the presence of an invariant chaotic repelling set. We stress that for class II maps the transient is absolutely non chaotic i.e. their transverse dynamics in tangent space is contracting at any time.

2.1 Finite Size Transverse Lyapunov Exponent

To quantitatively characterize the different transverse-space dynamics (i.e. the evolution of w^t shown in Fig. 1) for maps of class I and II, let us now introduce the Finite Size Transverse Lyapunov Exponent. The FSTLE, $\lambda_T(\epsilon)$, generalizes the concept of transverse Lyapunov exponent to finite value of the perturbation $jw^t = \epsilon$.

Following Aurell et al. [23] (see also Ref. [24]) we have defined the FSTLE as follows. We introduce a set of thresholds $\epsilon_n = \epsilon_0 k^n$ with $n = 1; \dots; N$, since on average a transverse expanding (resp. contracting) dynamics is expected in the desynchronized (resp. synchronized) regime, we choose $k > 1$ (e.g. $k = 2$)

for $\mu < \mu_1$ and $k < 1$ (e.g. $k = 1/2$) for $\mu > \mu_1$. First, starting from a random initial conditions we wait for x^t to relax onto its attractor. Then we initialize a second variable y^0 as $y^0 = x^0 + \delta_0$ by choosing an initial perturbation $\delta_0 < 0$ (resp. $\delta_0 > 0$) if $\mu < \mu_1$ (resp. if $\mu > \mu_1$), and let x^t and y^t evolve according to Eq. (1). Care should, of course, be taken to maintain y^0 within the interval of definition of the map. During the evolution we record the time, $(n; k)$, needed for y^t to pass for the first time from one threshold θ_n to the following one θ_{n+1} and also the value of $y^t = w_n$ at the moment of the passage. When the last threshold, θ_N , is reached the system is reinitialized with the above described procedure and this is repeated M times. The FSTLE is thus defined as

$$\tau(n) = \frac{1}{h(n; k)} \ln \frac{w_n}{\theta_n}; \quad (9)$$

where the average $h[n]$ is performed over the set of M different initial conditions. In the limit $\delta \rightarrow 0$ the FSTLE converges to τ . Notice that due to its definition, the FSTLE cannot measure at the same time expansion and contraction rates, i.e. we have limited the analysis only to consecutive contractions (resp. expansions) in the synchronized (resp. desynchronized) regime. This implies that the sign of $\tau(n)$ is always negative or positive in accordance with the investigated situation.

In Fig. 2 $\tau(n)$ versus δ is shown for different maps in the desynchronized regime. As expected, in all cases, for very small values of y^t the TLE is recovered. However, at larger values of y^t maps of the class II display an increase of the growth rate, i.e., $\tau(n) > \tau(0)$ for some finite value, while for maps of class I the FSTLE is monotonically decreasing with δ . $\tau(n)$ provides a quantitative measure of the strength of the nonlinear effects that, in maps of class II, may in principle overwhelm the linear mechanisms as pointed out in Ref. [30,25].

In Fig. 3 we report the behavior of $\tau(n)$ in the synchronized regime. Again, while for very small δ the (negative) TLE is recovered, at larger values the Bernoulli-like maps display an increase which is due to the jumps $O(1)$ of the transverse perturbation. A closer inspection of the small δ regime reveals that for the logistic map $\tau(n) \rightarrow \tau$ only for very small scales $\delta \sim 10^{-7}$, while for the skew tent map the asymptotic $\tau(n) \rightarrow \tau$ is never exactly reached. The latter convergence difficulties are probably due to the intermittent behavior along the transverse direction, in the proximity of the transition [3]. In the regime $\mu < \mu_1$ the finite time effects are less important and the asymptotic behavior is recovered for all the investigated maps.

The results presented in this subsection clearly indicate that finite scale instabilities can prevail on infinitesimal ones only for strongly nonlinear maps.

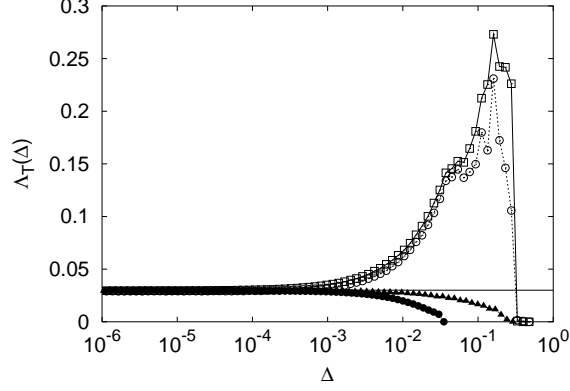


Fig. 2. $\Lambda_T(\Delta)$ vs Δ in the desynchronized regime for the Bernoulli map with $a = 1.5$ (empty circles), its continuous version (empty boxes) with $\epsilon = 10^{-4}$, the logistic map (filled circles) and the skew tent map (filled triangles). The coupling constants have been chosen in such a way that in all systems the transverse LE is equal to $\Lambda_T = 0.03$ (solid line).

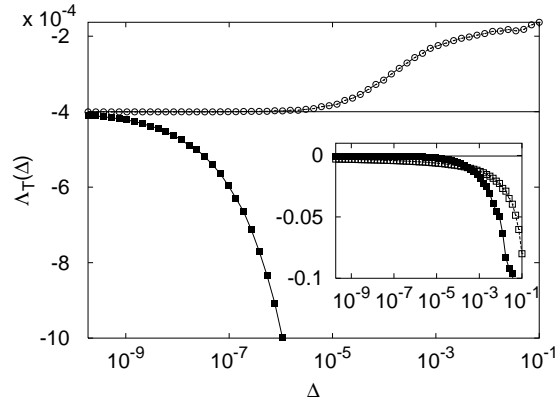


Fig. 3. $\Lambda_T(\Delta)$ vs Δ in the synchronized regime for the Bernoulli map at $a = 1.5$ (empty circles), the logistic map (filled boxes). The inset shows the logistic map (filled boxes) and the skew tent map (empty boxes). The straight lines correspond to the transverse LE, here $\Lambda_T = -4 \cdot 10^{-4}$ for all systems.

2.2 Statistics of the synchronization times

Notwithstanding the observed differences in the FSTLE, we found that the critical coupling for synchronization to occur is always given by (2) for both classes. This means that, at least for the case of two coupled maps, nonlinear effects do never modify the critical coupling. It is natural to wonder whether other observables related to the synchronization transition could be influenced by the presence of finite amplitude instabilities. As we shall show in this section, this is the case for the synchronization times statistics.

Let us define the synchronization time t_s , as the shortest time needed to $|w^t|$ for decreasing below a certain threshold ϵ , with the further requirement that

$j^t j < \tau$ for a sufficiently long successive time T_{st} . However, if the threshold value is small enough (e.g. 10^{-8} – 10^{-14}) essentially coincides with the first arrival time to the considered τ . The quantities of interest are the PDF's, $P(\tau)$, and their moments (we shall focus mainly on the first moment).

2.2.1 Class Maps

In Fig. 4 we show $P(\tau)$ for the logistic and the symmetric tent map. The main feature is the presence of an exponential tail at short times and the faster than exponential fall-off at long times. This means that synchronization times τ_{hi} are not observed. As a first result we derive, by following Ref. [6], an approximate analytical expression for $P(\tau)$, which is exact for the symmetric tent map.

Let us define $z^t = \ln |f^t|$ and consider its linearized evolution, from Eqs. (5) and (6) one obtains

$$z^{t+1} = z^t + \ln |f^0(u^t)| + \tau_{\text{st}} \epsilon_0 : \quad (10)$$

Formally the above equation can be applied only in the true linear regime, i.e. when $j^t j \neq 0$, so that it is not appropriate in the early stages of the evolution. However, as shown in Fig. 1, for maps like the logistic one, usually after a reasonably short transient, the linear regime sets in and the use of Eq. (10) is justified for the successive evolution. From Eq. (10) it is clear that $P(\tau)$ is related to the PDF $P(z)$ of the variable z and to that of the local multipliers $\ln |f^0(u^t)|$. The formal solution of Eq. (10) up to time N can be written as follows:

$$z^N = z^0 + \tau_{\text{st}} N + \sum_{i=0}^{N-1} \ln |f^0(u^i)| ; \quad (11)$$

where $\sum_{i=0}^{N-1} \ln |f^0(u^i)| = \sum_{i=0}^{N-1} \ln |f^0(u^i)|$. For sufficiently large N , large deviation theory tells us that the PDF of $\sum_{i=0}^{N-1} \ln |f^0(u^i)|$ takes the form $p(\tau) \sim \exp(-N g(\tau))$, being $g(\tau)$ the Cramér function [31], which is convex and has its minimum value at $g(\tau = 0) = 0$. It is now clear the distinction between the generic case in which $g(\tau)$ does not collapse onto a δ -function, and the non-generic one in which it does, as for the symmetric tent map and the logistic one at the Ulam point. In the former case the dynamics of z^t becomes a biased Brownian motion, with an average drift given by τ_{st} .

For the sake of simplicity, let us start from the tent map (Eq. (7) for $a = 1/2$), for which $\ln |f^0(u^t)| = \ln(2) - \tau_{\text{st}}$. In this case τ_{st} is simply given by:

$$\tau_{\text{st}} = \frac{z}{\langle j^t j \rangle} = \frac{\ln 2}{\langle j^t j \rangle} \quad (12)$$

and $P(\tau)$ can be directly related to $P(z)$. Since, in the proximity of the tran-

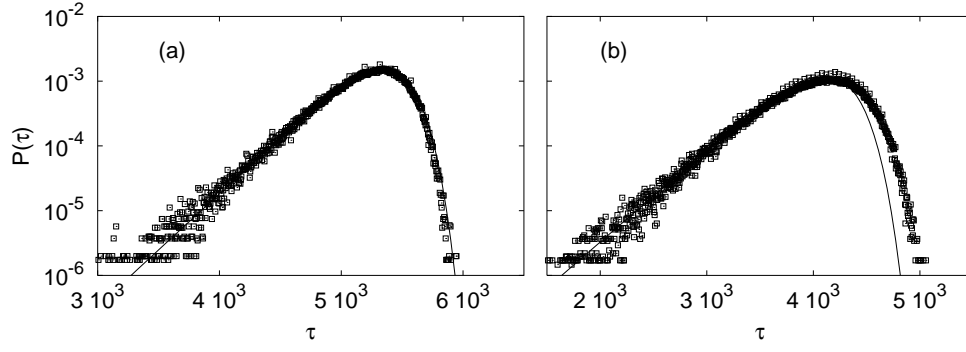


Fig. 4. $P(\tau)$ as a function of the synchronization time τ : (a) tent map for $\mu = (\mu_1) = 0.001$, the dashed line is the analytical expression (14); (b) logistic map for $\mu = 0.001$, the solid line refers to the expression (15) with $D = 0.82$ and $D^0 = 0.72$. In all cases the PDF have been obtained by averaging over 10^6 different initial conditions and by choosing $\epsilon = 10^{-12}$.

sition, $P(z = \ln |w|)$ assumes the form (analytically derived in Ref. [6]):

$$P(z) = \frac{2}{j_T j} e^z e^{-\frac{2}{j_T j} e^z}; \quad (13)$$

it can be easily obtained the related distribution

$$P(\tau) = 2e^{j_T j + \ln} e^{-\frac{2}{j_T j} e^{j_T j + \ln}}; \quad (14)$$

which perfectly agrees with the numerical results (Fig. 4a).

Unfortunately the (short time) multiplier statistics of the logistic map is nontrivial, impeding a straightforward derivation of $P(\tau)$. However, we numerically observed that $P(w) \sim e^{D w}$ ($w = \exp(z)$) with D almost constant in a neighborhood of the transition (namely, $D = 0.82 \pm 0.02$ for $0.01 \leq \mu \leq 0.01$). This implies that

$$P(\tau) = 2e^{D j_T j + C} e^{-\frac{2}{j_T j} e^{D j_T j + C}}; \quad (15)$$

which is in fairly good agreement with the numerically evaluated PDF (Fig. 4b). Notice that C is not simply given by $D \ln$, and a fitting procedure is needed. We found $C = D^0 \ln$, with $D^0 = 0.72; 0.70$ and 0.65 for $\epsilon = 10^{-3}; 10^{-4}$ and 10^{-5} , respectively.

The above reported results allow us also to predict the scaling of the average synchronization time $\bar{\tau}$ with μ in the proximity of the synchronization transition. In particular, for the symmetric tent map the following expression can be derived

$$\bar{\tau} = \int_0^{\infty} \tau dP(\tau) = \frac{E_1 \frac{2}{j_T j}}{j_T j}; \quad (16)$$

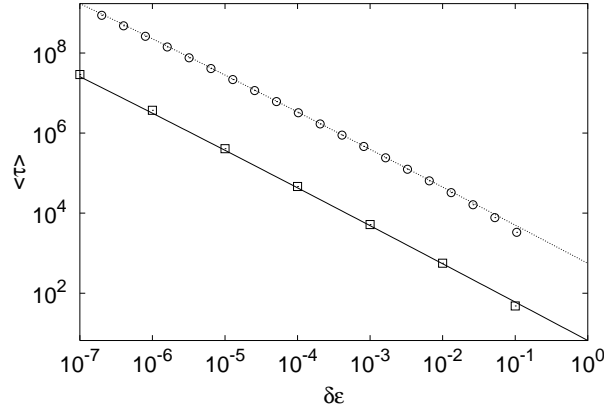


Fig. 5. h_i vs $\epsilon = \delta\epsilon$ for the tent map (empty boxes) and the logistic one (empty circles). The continuous line is the prediction (17) with $\epsilon = 10^{-12}$, the dotted one is obtained by a best fit of the form $h_i = (a + b \ln(\epsilon))\epsilon$, with $a = 5.58$ and $b = 0.24$. The data of the logistic map have been shifted by a factor 100 for plotting purposes.

where [32]

$$E_1(x) = \sum_{n=1}^{\infty} \frac{1}{x} \frac{d^n}{dx^n} \frac{e^{-y}}{y} = \ln x + \sum_{n=1}^{\infty} \frac{(-1)^n x^n}{n! n};$$

being $\gamma = 0.57721 \dots$ the Euler-Mascheroni constant. Since $2 = j_T j - 1$, approximately we have

$$h_i \sim \frac{\ln \epsilon + \ln(j_T j - 8)}{j_T j}; \quad (17)$$

where $j_T j - 2e^0 = 4$ (being $e^0 = \ln 2$). Note that (17) is in perfect agreement with the numerical results for the tent map (see Fig. 5). For the logistic map, a similar dependence on ϵ , namely $h_i = (a + b \ln(\epsilon))\epsilon$, has been found. The interesting point in (17) is the logarithmic correction to the scaling $h_i \sim \epsilon^{-1}$, which would have not been predicted by a naive guess based on (12).

We now briefly discuss the generic situation (see Chap. 13 of Ref. [3] for more details). As mentioned above, $z^t = \ln j^t j$ performs a biased Brownian motion, so that computing $P(\epsilon)$ amounts to evaluate the distribution of the first passage times to a threshold of a Wiener process with drift that, as a standard result of stochastic process theory, is given by an inverse Gaussian density [26] that for long times becomes

$$P(\epsilon) \sim \frac{3}{2} \epsilon^{-3/2} e^{-\frac{3}{2} \epsilon} \quad \text{with} \quad \epsilon = \frac{2}{T}; \quad (18)$$

where the quadratic dependence from the TLE comes from the diffusive dynamics of the perturbation.

2.2.2 Class II maps

For class II maps the situation is completely different. For both the continuous Bernoulli map (Fig. 6a) and the discontinuous Bernoulli shift (Fig. 6b) we observe that for $\mu > \mu_1$ the PDF's are characterized by an exponential tail at large x , similar to Poissonian distributions. Moreover, we also observe that the PDF's, once rescaled as $P(x) \rightarrow P(x/\mu)$, and reported as a function of $x = (h_i - h_{i-1})/\mu$ (where $\mu = h_{i-1} - h_i$) collapse onto a common curve in the proximity of the transition. These results are particularly striking in the case of the Bernoulli map for which naively one would have expected a complete similarity with the tent map, since its multiplier $f'(x) = r$ is also constant. Here the presence of strong nonlinear effects makes the transient time statistics to be dramatically different from (14). Indeed, as seen in Fig. 1, w_t is subject to noticeably nonlinear amplifications induced by the (almost) discontinuities in the map. Therefore, the expression (10) is no more appropriate to describe the dynamics of $z_t = \ln |w_t|$ and its full nonlinear dynamics has to be taken into account. The latter is characterized by the fact that, with a finite probability, $|w_t|$ can jump to $O(1)$ values at any time during the transient preceding the synchronization, even if the transient is not chaotic.

This idea can be better clarified and its consequences on the $P(x)$ better appreciated by considering a simple stochastic model for the dynamics of the transverse variable at $\mu > \mu_1$. This model was originally proposed in Ref. [33], and reads as

$$w^{t+1} = \begin{cases} 1 & \text{with probability } p = e^{\tau w^t} \\ e^{\tau w^t} w^t & \text{with probability } 1 - p \end{cases}; \quad (19)$$

where $\tau < 0$ and w^t is a shorthand notation for $|w^t|$ with probability. The underlying idea is very simple: the transverse perturbation w^t is usually contracted, but with probability proportional to its amplitude can be re-expanded to $O(1)$ values, in agreement with the numerical observations. The jumps occur when x^t and y^t are close but located at the opposite sides of the (almost) discontinuity.

For this simple model, it is possible to derive the corresponding probability density $P(x)$, which displays the same peculiar features of the PDFs reported in Figs. 6a and 6b. In particular, the long time tail. First, notice that the probability that an initial perturbation w_0 is never amplified to $O(1)$ up to time t is given by

$$Q(t; w_0) = \prod_{n=1}^t [1 - w_0 e^{\tau^n}]! \quad Q(w_0) = \lim_{t \rightarrow \infty} \exp \left(- \sum_{k=1}^{\infty} \frac{w_0^k e^{j \tau^k}}{k (1 - e^{j \tau^k})} \right); \quad (20)$$

Interestingly, for $-1 < \tau < 0$ the quantity $Q(w_0)$ is always positive and

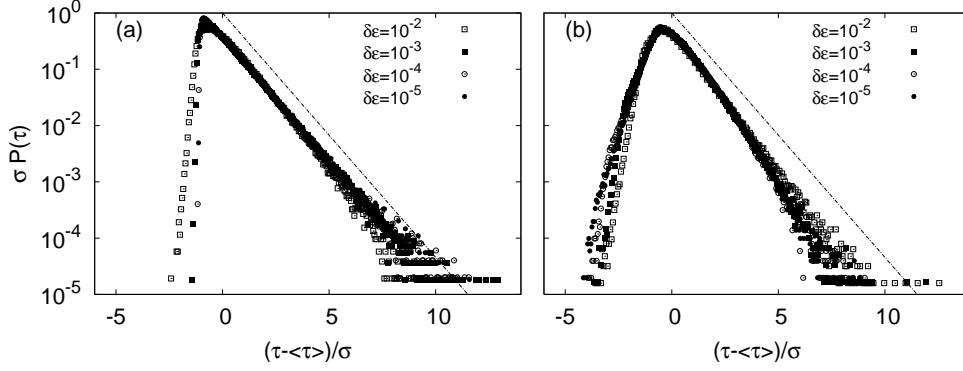


Fig. 6. (a) P as a function of $(\tau - \langle \tau \rangle) / \sigma$ (where $\sigma = \sqrt{\frac{1}{h^2} \langle (\tau - \langle \tau \rangle)^2 \rangle - \langle \tau - \langle \tau \rangle \rangle^2}$) for the continuous Bernoulli shift map (8) with $a_1 = 1$ and $\epsilon = 10^{-3}$ at different distances, $\delta \epsilon$, from the critical coupling. Note the fairly good collapse, indicating a common decay as e^{-x} (dashed line). The collapse is however only approximate near the peak. (b) Same as (a) for the Bernoulli map with $r = 2$ at different distances from the critical coupling. The dashed line gives e^{-x} .

strictly smaller than 1 for any perturbation $|j_0| > 0$, i.e. the probability that a perturbation of amplitude $|j_0|$ can be amplified is finite at any time.

The PDF of the times needed to observe $w =$ can be factorized as

$$P(\tau) = G(\tau - \langle \tau \rangle) Q(n; 1); \quad (21)$$

where $G(\tau - \langle \tau \rangle)$ is the probability to receive a kick at time $\tau - \langle \tau \rangle$, and $Q(n; 1)$ is the probability of not being amplified for the following n steps, where n is given by

$$n = \lfloor \ln |j_0| / \ln |j_T| \rfloor$$

As shown in Ref.[33] $G(x) \sim \exp(-x)$, and therefore at large τ 's Eq. (21) can be rewritten as

$$P(\tau) / Q(n; 1) \exp[-(\tau - \langle \tau \rangle)] \quad (22)$$

that confirms the Poissonian character of the PDF $P(\tau)$ for the maps of class II. By properly normalizing Eq. (22), one obtains $h(\tau) = 1 - \ln |j_T| / \ln |j_0|$ that is in good agreement with the numerical results for the Bernoulli map (in particular, we considered $r = 2$ and $\epsilon = 10^{-12}$). Moreover, in the interval $\tau^2 \in [10^{-5}; 10^{-2}]$ we found that the decay rate of the PDF is directly proportional to the TLE, i.e. $0.2 |j_T|$, this should be contrasted with the quadratic dependence found in the case of class I maps, see Eq. (18).

2.3 Synchronization transition

We conclude the investigation of two coupled maps by studying the nature of the transition. For this purpose let us introduce the order parameter $\langle \tau \rangle$

defined as (see also Ref. [34]):

$$\langle \rho \rangle = \lim_{N \rightarrow \infty} \frac{1}{N} \lim_{T \rightarrow \infty} \frac{1}{T} \sum_{i=1}^N \sum_{t=1}^T \langle \mathbf{w}^{t+T_w} \rangle; \quad (23)$$

i.e. for each value of the coupling ρ , one considers N different random initial conditions and each one is iterated for a transient T_w after which the time average of $\langle \mathbf{w}^t \rangle$ over a time lapse T is considered and further averaged over all the initial conditions. The value of the coupling giving the synchronization transition is then implicitly defined as $\langle \rho \rangle_{n1} = 0$. In principle, $\langle \rho \rangle_{n1}$ may differ from ρ_1 defined by (2), since this expression is valid only within a linear approximation formalism. In Fig. 7 we show the behavior of the order parameter

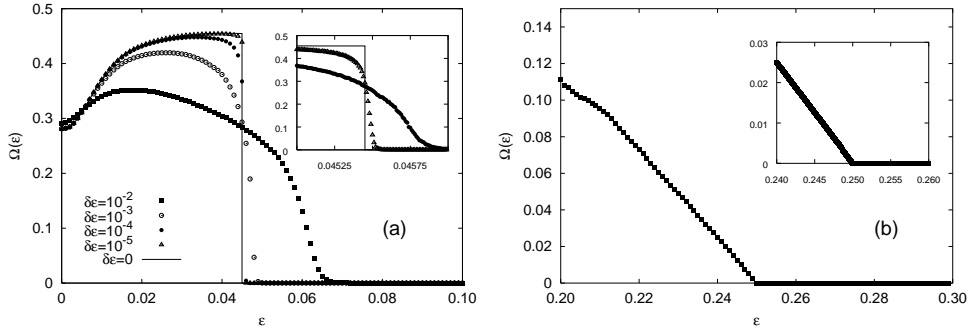


Fig. 7. (a) $\langle \rho \rangle$ vs ρ for the Bernoulli map with $r = 1:1$ and its continuous version (8) for different values of $\delta \epsilon$. For the Bernoulli map one has that according to (2) $\rho_1 = 0.0454545\dots$. The order parameter is computed according to (23) averaging over $N = 10^3$ different random initial conditions, discarding the first 10^6 iteration and averaging over the following 10^5 iterations. $\langle \rho \rangle$ has been estimated with an ρ -resolution 10^{-3} . The inset shows an enlargement of the critical region done with a coupling resolution 10^{-4} , the same number of initial conditions and a longer integration transient $T_w = 3 \cdot 10^6$ iterations. (b) The same for the logistic map at the crisis. Here (2) predicts $\rho_1 = 0.25$. The blow up of the critical region (in the inset) shows that the transition is continuous. Note also that for $\rho = 1$ we observe $\langle \rho \rangle = 1$.

eter (23) as a function of ρ for both classes of systems. Two observations are in order. First, the transition to the synchronized state always occurs at the critical coupling defined by (2) (i.e. $\rho_{n1} = \rho_1$). Second, the transition is continuous for the Logistic map (simulations show that also the tent map, which belongs to the same class, has a continuous transition) and discontinuous for the Bernoulli shift. This confirms the results reported in Ref. [34]. However, since the transition for the continuous version of the Bernoulli shift map (8) is steep but clearly continuous (see the inset of Fig. 7a), this does not seem to be a generic property for all the maps of class II.

The behavior of the Bernoulli shift map can be easily understood by consid-

ering the map controlling the dynamics of w^t , i.e.

$$w^{t+1} = \begin{cases} (1 - 2\mu)rw^t & \text{if } x^t \in I_0, y^t \in I_0 \\ (1 - 2\mu)(rw^t + 1) & \text{if } x^t \in I_1, y^t \in I_1 \\ (1 - 2\mu)(rw^t + 1)x^t & \text{if } x^t \in I_0, y^t \in I_1 \\ (1 - 2\mu)(rw^t - 1)y^t & \text{if } x^t \in I_1, y^t \in I_0 \end{cases} \quad (24)$$

being $I_0 = [0 : 1-r]$ and $I_1 = [1-r : 1]$. From the above expression, it is evident that the attractor in the $(w^t; w^{t+1})$ plane has always a finite width along the transversal direction, unless $x^t = y^t$. This explains the discontinuity observed at μ_1 . In the continuous map (8) the attractor in the plane $(w^t; w^{t+1})$ has a "transverse" width that decreases continuously to zero for $\mu \rightarrow \mu_1$. In conclusion, the discontinuity in the transition is a pathology of the Bernoulli map, and possibly of other discontinuous maps.

The order parameter (23) can be seen as the time average, once discarded an initial transient, of the following quantity

$$W(t) = \langle w^t \rangle \quad (\text{for } t \gg 1); \quad (25)$$

where $\langle \rangle$ indicates the average over many different initial conditions. Once w is initialized 0 (1), depending on whether μ is smaller or larger than μ_1 two different asymptotic behavior are observed. In the desynchronized regime, obviously $W(t)$ goes to a finite value (μ), while above the synchronization transition $W(t) \rightarrow 0$ with a decay law determined by the nature of the considered maps. For class I maps, the decay is ruled by the TLE: $W(t) \sim \exp(\tau t)$ with $\tau < 0$. For class II maps $W(t)$ shows an initial exponential decay $\exp(-\tau t)$ (with $\tau > 0$), due to the effect of the resurgences averaged over many different initial conditions, followed by a final linear decay $\exp(-\tau t)$.

The nonlinear rate can be simply related to the exponential tail of the PDF of the first arrival times, by assuming (as indeed observed) the following decay $P(t) \sim \exp[-(\frac{\ln t}{j_T})]$. Since $W(t)$ is the average amplitude value of the w^t at time t , one has

$$W(t) = \int_0^1 P(t) dt / \int_0^1 P(t) dt = e^{-\frac{\ln t}{j_T}} = e^{-t \frac{\ln t}{j_T}} = e^{-t \frac{1}{j_T}} : (26)$$

The above result tells us that $\tau = -\frac{1}{j_T}$ (if the integral does not diverge, i.e. if $j_T > 0$). This is confirmed by numerical checks.

3 Coupled maps with power law coupling

In this section we analyze high dimensional systems, namely the power-law coupled maps defined in Eq. (3). In particular, for class II maps we shall show that there exist situations where, due to the nonlinearities, the synchronization time diverges exponentially with the number of maps. As a consequence, the transition takes place at a (nonlinear) critical coupling κ_{n1} larger than the linear value κ_1 . A similar phenomenon has been observed for GCM's with nonlinear coupling, where the synchronization time divergence is due to a chaotic transient [7]. Chaotic transients, diverging exponentially with the number of coupled elements, have been reported also for spatially extended reaction-diffusion systems [35] and for diluted networks of spiking neurons [36]. However, the emphasis of our work is on non-chaotic transients similar to the stable-chaos phenomenon [28].

Let us start by reviewing the linear theory developed in Ref. [10], which is able to account for the synchronization transition of class I maps.

3.1 Lyapunov Analysis

When nonlinear effects are not sufficiently strong, excluding the pathological cases of chaotic transients, the critical coupling for observing the synchronization transition can be predicted by computing the Lyapunov spectrum. In particular, since above the synchronization transition the transverse Lyapunov exponent coincides with the second Lyapunov exponent, λ_2 , it suffices to evaluate the dependence of the latter on κ .

In order to compute the Lyapunov spectrum of the model (3), it is necessary to consider the tangent space evolution:

$$\mathbf{x}_i^{t+1} = (1 - \kappa) \mathbf{f}^0(\mathbf{x}_i^t) \mathbf{x}_i^t + \frac{\kappa}{L} \sum_{k=1}^L \frac{\mathbf{f}^0(\mathbf{x}_{i-k}^t) \mathbf{x}_{i-k}^t + \mathbf{f}^0(\mathbf{x}_{i+k}^t) \mathbf{x}_{i+k}^t}{k} : \quad (27)$$

In Ref. [10] it has been shown that the full Lyapunov spectrum can be easily obtained for the Bernoulli map:

$$\lambda_k = \ln r + \ln |1 - \frac{\kappa}{L}| + \frac{1}{L} \ln b_k ; \quad (28)$$

where

$$b_k = 2^{\frac{\kappa}{L}} \frac{\cos(2\pi \frac{(k-1)m}{L})}{m} \quad k = 1, \dots, L : \quad (29)$$

In this notation the maximal Lyapunov exponent is given by $\lambda_1 = \ln r$ and the second Lyapunov exponent is λ_2 .

For generic maps it is still possible to obtain the Lyapunov spectrum in an analytical way, but only in the synchronized state, by substituting $\ln r$ with the maximal LE of the single uncoupled map f_0 in (28).

From a linear analysis point of view one expects that the synchronization transition has to occur when $\lambda_2 = 0$. Therefore, the following expression for the critical line in the $(\epsilon; \alpha)$ -plane can be derived:

$$\lambda_2 = \lambda_1 - \epsilon \sum_{m=1}^L \frac{2}{m} \frac{X_1^0 \cos(2\pi m/L)}{A} : \quad (30)$$

As shown in Ref. [10] this prediction is well verified for the logistic map, which is here used as a benchmark for our codes. Let us conclude this short review by noticing that in the limit $L \rightarrow 1$ synchronization can be achieved only for $\alpha < 1$ [10]. Therefore we shall limit our analysis to this interval.

3.2 Nonlinear synchronization transition

Let us now study the critical line for class II maps, exemplified by the Bernoulli shift map and its continuous version. First of all we introduce the main observables and the numerical method employed to determine it.

A meaningful order parameter for the transition is represented by time average of the following mean field quantity :

$$S(t) = \frac{1}{L} \sum_{i=1}^L \mathbf{x}_i^t \cdot \bar{\mathbf{x}}^t; \quad \bar{\mathbf{x}}^t = \frac{1}{L} \sum_{i=1}^L \mathbf{x}_i^t : \quad (31)$$

This can be operatively defined as follows : firstly the system (3) is randomly initialized and iterated for a transient time T_w proportional to the system size L , then the time average of $S(t)$ is computed over a time window T , i.e. $\langle S \rangle_T = \frac{1}{T} \int_{t=1}^T S(t) dt$. Finally the state of the system is defined as synchronized if $\langle S \rangle_T < \epsilon$, being a sufficiently small value (10^{-8} - 10^{-10} is usually enough). The coupling value corresponding to the synchronization transition is then obtained by using a bisection method: chosen two coupling values across the transition line one corresponding to a desynchronized state (α_d) and the other to a synchronized case (α_s) a third value is selected as $\alpha_m = (\alpha_d + \alpha_s)/2$. If at this new coupling value the system synchronizes (resp. not synchronizes) α_m is identified with the new α_s (resp. α_d). The procedure is then repeated until $(\alpha_s - \alpha_d) < \epsilon$ (in our simulations $\epsilon = 10^{-3}$ - 10^{-5}). Finally the critical coupling is defined as $\alpha_{c1} = (\alpha_s + \alpha_d)/2$. The algorithm, tested on the logistic

map, was able to recover (30) with the required accuracy. In general one has that, once fixed α , ρ_{n1} will be a function of T_w for a given L .

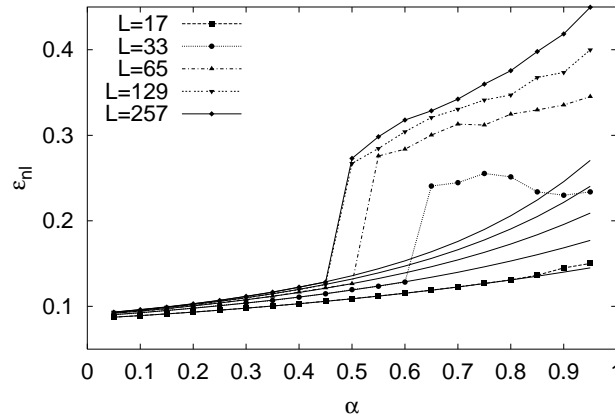


Fig. 8. Synchronization transition lines for the Bernoulli shift map with $r = 1:1$ at $L = 17; 33; 65; 129; 257$. The solid lines are the analytically estimated "linear" transition values Eq. (30), while the symbols refer to the numerically obtained values. We used $T_w = 10^5 L$, $T = 10^3 L$, $\epsilon = 10^{-8}$ and $\delta = 10^{-3}$.

In Refs. [7,10] it has been employed as a synchronization indicator the time average of the following mean-field quantity:

$$R^t = \frac{1}{L} \sum_{j=1}^L e^{2 i x_j^t} : \quad (32)$$

We have verified that this indicator gives results completely analogous to ρ_{n1} in all the considered cases.

In Ref. [10] the authors have reported for logistic coupled maps a very good agreement between ρ_{n1} given by (30) and ρ_{n1} estimated via $\langle R^t \rangle_T$. However, this is not the case for the Bernoulli map, as shown in Fig. 8. In this case (depending on the slope of the map r , on α and on the chain length L) strong disagreements between the linear transition line given by ρ_{n1} and the numerically obtained values are observed. These disagreements are typical of class II maps. Since the nonlinear effects locally desynchronize the system even if $\alpha < 0$, in general $\rho_{n1} < 1$.

In obtaining the data reported in Fig. 8, the cpu time restrictions forced us to employ a large but somehow limited transient time (namely, $T_w = 10^5 L$). Therefore, we checked for the dependence of the results on T_w for fixed L . In particular, we measured ρ_{n1} for two α -values only (namely, $\alpha = 0.3$ and 0.8) for several chain lengths and transient times. This analysis has been performed for the logistic map at the crisis, for the Bernoulli shift map with $r = 1:1$ and for its continuous version. The results are reported in Fig. 9. For the logistic map we found that, for any value of L and α , a relatively small value of T_w ($< 10^4$)

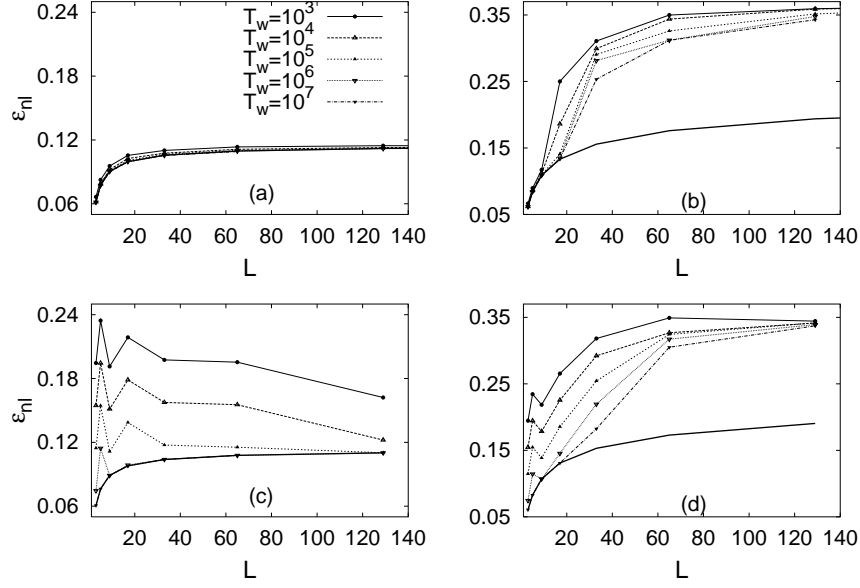


Fig. 9. ϵ_{n1} as a function of L for different T_w in $10^3 \dots 10^7$ for the continuous Bernoulli shift map with $r = 1:1$ and $\beta = 0.3$ (a) and $\beta = 0.8$ (b). The same for the Bernoulli shift with $r = 1:1$ for $\beta = 0.3$ (c) and for $\beta = 0.8$ (d). The continuous solid lines are the theoretical values obtained in the linear analysis framework (30).

was sufficient to observe a clear convergence of ϵ_{n1} to the linear value ϵ_1 . This is also the case of the Bernoulli map and its continuous version for $\beta = 0.3$ (though as one can see in Fig. 9c the discontinuous map is characterized by a slightly slower convergence than its continuous version). On the contrary for $\beta = 0.8$ with $L \leq 21$ we were unable to observe synchronization even for $T_w = 10^7 L$, while at $T_w = 10^4 L$ the logistic map had already converged to ϵ_1 . Summarizing for $r = 1:1$ we found that for $\beta \leq 0.5$ the Bernoulli shift map and its continuous version always converge toward the linear critical value, while for $\beta > 0.5$ at increasing L the critical coupling ϵ_{n1} becomes more and more independent of the transient time T_w (see the right of Fig. 9 for $L = 129$). However, for a smaller value of r and for large L (we investigated the case $r = 1:01$ and $L = 101; 501$) we observed $\epsilon_{n1} > \epsilon_1$ for any value of $\beta \in [0; 1]$. In particular, we stress that also in the globally coupled case (corresponding to $\beta = 0$) we have clear evidences that $\epsilon_{n1} > \epsilon_1$. This is due to the fact that for $r \neq 1$ nonlinear finite amplitude instabilities becomes more and more predominant with respect to the mechanism of linear stabilization (see [30, 29] for more details).

On the basis of the previous results, it is natural to conjecture that in the limit $L \rightarrow \infty$ the non-linear transition is well defined, i.e. that the limit

$$\epsilon_{n1}(\beta) = \lim_{T_w \rightarrow \infty} \lim_{L \rightarrow \infty} \epsilon_{n1}(\beta; L; T_w): \quad (33)$$

exists and is typically larger than $\epsilon_1(\beta) = \lim_{L \rightarrow \infty} \epsilon_1(\beta; L)$. Note that in the

above expression the order of the two limits is crucial, we expect that performing at fixed L the limit $T_w \rightarrow 1$ we should always observe a convergence to μ_1 . However, as shown in the following, the times to reach synchronization may diverge exponentially fast with L in the region just above μ_1 making rapidly infeasible this limit.

3.3 Synchronization Times

As for the case of two coupled maps, we study now the synchronization time statistics. In particular, we consider the system above the linear transition line $\mu > \mu_1$ and measure the first passage times needed for $S(t)$ (32) to decrease below a given threshold ϵ . In this way we determine the corresponding PDF and the related moments.

In the high dimensional case, it is fundamental to analyze the dependence of the synchronization time on the system size L . However, as reported in Eq. (30), the critical value μ_1 itself depends on L . Therefore to perform a meaningful comparison of systems of different sizes we considered situations characterized by the same linear behavior in the transverse space, i.e. having the same value of μ_2 . This means that for each length L we chose the coupling strength according to

$$\mu(\mu_2) = \mu_1(L) \frac{e^{\mu_2} - e^{\mu_1}}{e^{\mu_2} - 1} : \quad (34)$$

Further tests performed at different lengths but at a fixed distance $\mu - \mu_1(L)$ from the critical line give essentially the same results.

As shown in Fig. 10a, for the logistic map (but these results can be extended to all maps belonging to class I, see Fig. 10b) the PDF's of the synchronization times obtained at constant μ_2 display a very weak (almost absent) dependence on the system size, and are qualitatively similar to that found for two coupled maps (compare Fig. 10a with Fig. 4). Moreover, measurements of the average synchronization times \bar{t} , done by fixing the "distance" $\mu - \mu_1$ from the critical line, exhibit a clear tendency to saturate for increasing L (Fig. 11). Therefore, in the limit $L \rightarrow \infty$ the synchronization time will not diverge.

For the maps of class II the situation is different. Here, as shown in Fig. 10c, for values of μ sufficiently small $P(t)$ is weakly dependent on the system size as found for the logistic map. On the other hand, by considering more local couplings (e.g. $\mu = 0.8$ in Fig. 10d), the tail of the PDF becomes more and more pronounced as the system size increases. Results obtained by fixing the distance from the critical coupling instead of the value of the TLE display qualitatively similar features.

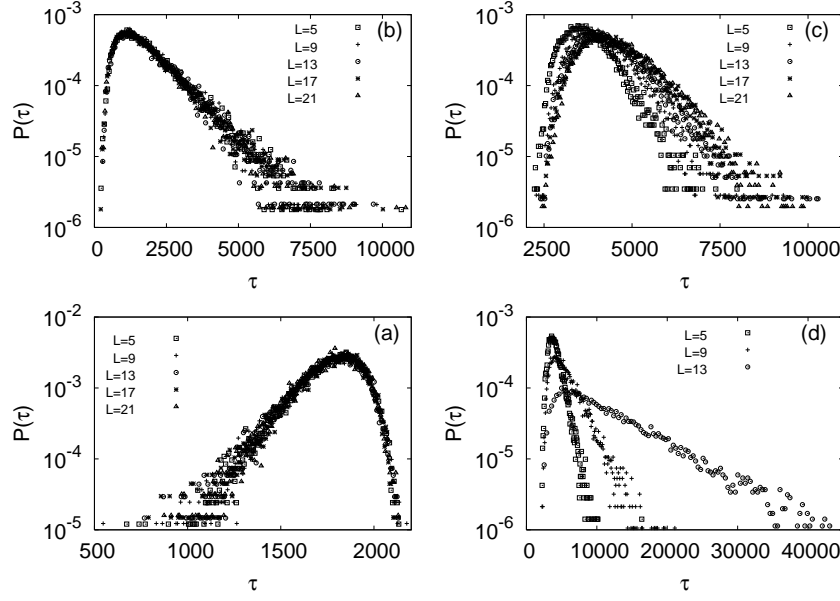


Fig. 10. $P(\tau)$ vs τ for different system sizes (see label) at fixed $\alpha_2 = 0.01$ for different maps: (a) logistic map at the crisis with $\alpha = 0.3$ (for $\alpha = 0.3$ we obtained qualitatively similar results); skew tent map (7) with $a = 2/3$ (b); Bernoulli shift map with $r = 1.1$ for $\alpha = 0.3$ (c) and $\alpha = 0.3$ (d). In the latter case sizes larger than $L = 17$ were not drawn for the sake of clarity of the plot. The PDF's have been obtained in all cases by considering 10^4 different initial conditions and with $N = 10^{12}$.

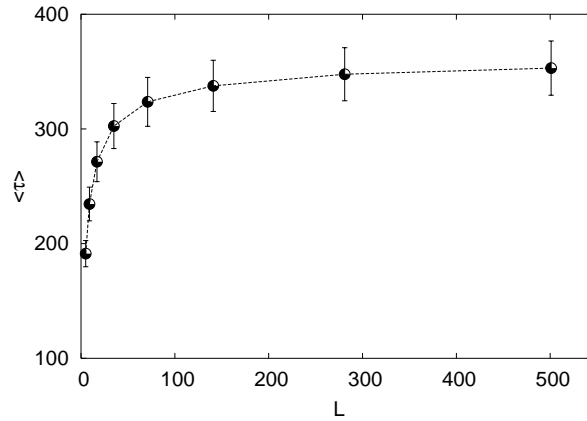


Fig. 11. Average synchronization time, h_i , as a function of the system size L for the logistic map at the crisis with $\alpha = 0.6$ estimated at a fixed distance from the linear threshold $\alpha = 0.05$. Data have been averaged over 10^5 initial conditions with $N = 10^{12}$.

This picture is further confirmed by examining h_i as a function of L for fixed α_2 (i.e. by choosing α according to (34)). As one can see in Fig. 12, h_i displays a dramatic dependence on L . In particular, at $\alpha_2 = 0.01$ (see the inset of Fig. 12) h_i grows exponentially with L , while a power-like scaling is observable for $\alpha_2 = 0.05$, at least for the chain lengths we could reach. Deeper

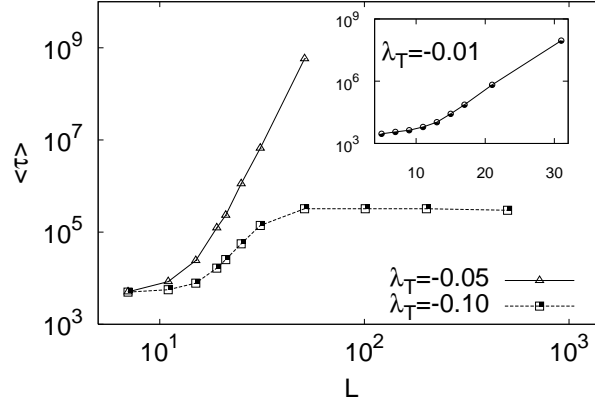


Fig. 12. Average synchronization times \bar{t}_s as a function of L for the Bernoulli map with $r = 1:1$ and $\alpha = 0.8$ for various values of the second Lyapunov exponent (see label). The inset shows the case of $\lambda_T = -0.01$ in linear scale. Data have been averaged over 10^4 initial conditions and $\alpha = 10^{-12}$.

inside the "linear" synchronization region, i.e. for $\lambda_T = 0.1$, we observed a saturation of \bar{t}_s with the system size. It is worth stressing here that for $\alpha = 0.3$ and $r = 1:1$, where no appreciable discrepancies between τ_{n1} and τ_1 have been observed, \bar{t}_s saturates for large L . Nevertheless the corresponding PDF exhibits the usual tail at long times characteristic of maps of class II but with weak dependence on L (see Fig. 10c). Notice also that, in principle, the transition from the exponential dependence to the saturation can be used to estimate τ_{n1} (see Ref. [8]), however for the present model a systematic study of this aspect is infeasible due to the required computational resources.

We thus found clear indications that a nonlinear synchronization transition can be observed for class II maps when finite size nonlinear instabilities are sufficiently strong to overcome the effects of stabilization associated with the local linear dynamics and to the spatial coupling. This suggests that nonlinear effects tend to decouple the single units of the chain. This decoupling can be indeed related, by means of the following simple argument, to the observed exponential divergence with L of the synchronization times at $\tau_{n1} > \tau > \tau_1$. Synchronization happens when the difference $s_i^t = |x_i^t - x_j^t|$ is contracted forever in each site until $S(t) = s_i^t$ decreases below threshold. The probability that for a single site the initial difference $s_i^0 = w_0$ will be never amplified to $O(1)$ is given by $Q(w_0) < 1$ (see Eq. (20)), therefore by assuming that each site is completely decoupled from its neighbors the probability of contraction for the whole chain is given by $p = Q^L(1) = \exp[L \ln Q(1)]$ (for simplicity we set $w_0 = 1$ without loss of generality). And the probability that the system settles onto this "contracting" state after n steps is

$$P_n = (1 - p)^{n-1} p = \exp(-np) \quad (35)$$

this quantity represents a good approximation of $P(\tau)$. Therefore one expects a

Poissonian decay for the PDF of the synchronization times with an associated average time $\langle \tau \rangle = 1/p / \exp [L \ln(1-Q(1))]$ exponentially diverging with the chain length, as indeed observed.

3.4 Properties of the transitions

Let us now characterize the synchronization transition in the spatially extended model (3) within the framework of non-equilibrium phase transitions. A similar parallel was recently established in a series of works concerning synchronization of two replicas of CML's with nearest neighbor coupling [8,9,33,37]. In these studies it has been shown that the synchronization transition is continuous and belongs to the Multiplicative Noise (resp. Directed Percolation) universality class depending on the linear (resp. nonlinear) nature of the prevailing mechanisms. In both cases one observes a transition from an active phase (characterized by $hSi_T = S_0 > 0$) to a unique absorbing state (identified by $hSi_T = 0$). We indicated with S the order parameter, however for sake of clarity it should be said that for two replicas of a CML this corresponds to $S(t) = \frac{1}{P} \sum_{i=1,L} \mathbf{x}_i^t \cdot \mathbf{y}_i^t$ and is not given by expression (32) used in the present paper for characterizing self synchronization. The rationale for using the same symbol is that the two definitions embody essentially the same information: $\langle S \rangle_T$ is a measure of the density of non synchronized (active) sites.

In the proximity of the transition (if continuous) the scaling behavior of the saturated density S_0 of active sites is given by

$$S_0 \sim (\mu_c - \mu); \quad \text{for } \mu < \mu_c; \quad (36)$$

while at the critical point $\mu = \mu_c$ the density of active sites scales as $S(t) \sim t^{-\beta}$ and the average synchronization time diverges as

$$\langle \tau \rangle \sim L^z; \quad (37)$$

We denote as μ_c the critical coupling to avoid at this stage distinctions between linearly and nonlinearly driven synchronization. Since continuous non-equilibrium phase transitions are typically characterized by three independent critical exponents, once $(\beta; \nu; z)$ are known all the other scaling exponents can be derived [22].

Let us now analyze CML's with power-law coupling (3). We start with class I maps, for which the transition is completely characterized by the linear dynamics, i.e. $\mu_c = \mu_1$. In particular, we consider the logistic maps at the Ulam point for three different α -values (namely, $\alpha = 0.1; 0.3$ and 0.6). The first observation is that the critical properties of the model seem to be independent of α : we measured exactly the same critical exponents for the all α values,

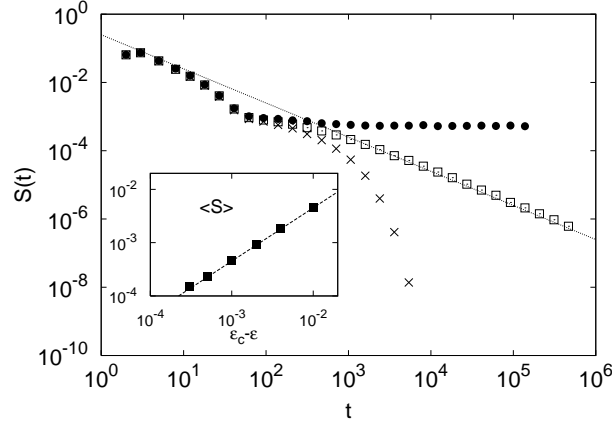


Fig. 13. Temporal evolution of the order parameter $S(t)$ for $\epsilon = \epsilon_c - 10^{-3}$ (filled circles) $\epsilon = \epsilon_c$ (empty boxes) and $\epsilon = \epsilon_c + 10^{-3}$ (crosses). The solid straight line displays the power law decay t^{-1} . Data refer to the logistic map with $\beta = 0.1$ and $L = 501$ and are obtained after averaging over 1;500 – 3;000 initial conditions. In the inset the average value of the order parameter $\langle S \rangle$ as a function of $\epsilon_c - \epsilon$ is reported. The straight line shows the scaling behavior $(\epsilon_c - \epsilon)^1$. Data refer to the logistic map with $\beta = 0.3$ and $L = 501$ the average is performed over 1;000 different initial conditions.

namely $\beta = 1$, $\gamma = 1$ (see Fig. 13) and $z = 0$ (see Fig. 11). These exponents coincide with the mean-field exponents reported in Ref. [38] for a model of anomalous Directed Percolation (DP). The model differently from standard DP considers the spreading of epidemics in the case of long-range infection, namely in one spatial dimension the probability distribution for a site to be infected at distance r decays as $1/r^{1+\beta}$. The critical behavior of this model can be obtained by considering a Langevin equation with power-law decaying spatial coupling for the coarse grained density of infected sites. In Ref. [38], the authors found that the critical exponents vary continuously with β , but below a critical value ($\beta_c = 1/2$ in 1d) the exponents coincide with the corresponding mean-field results, namely $\beta_{MF} = \gamma_{MF} = 1$ and $z_{MF} = 0$. In the limit $\beta \rightarrow 0$ the latter exponents are identical to the ones we have found for the logistic coupled maps. In the following we shall give an argument to explain these similarities and differences.

As shown in Refs. [8,9,33,37] there is a deep connection between the synchronization problem for two replicas of a diffusively coupled CML and nonequilibrium phase transitions. Indeed there the difference field $d_i^t = x_i^t - x_j^t$ can be mapped onto the density of infected (active) sites and an appropriate Langevin equation describing the evolution of d_i^t can be derived in proximity of the transition [20]. In our case of CMLs with power-law coupling we expect that the corresponding Langevin equation for the spatio-temporal coarse grained defect density $s_i^t = x_i^t - x_j^t$ should contain a long-range interaction with a power law spatial coupling decaying with an exponent β . Therefore, in the proximity of the transition, it seems natural to map the dynamics of (3) onto the model

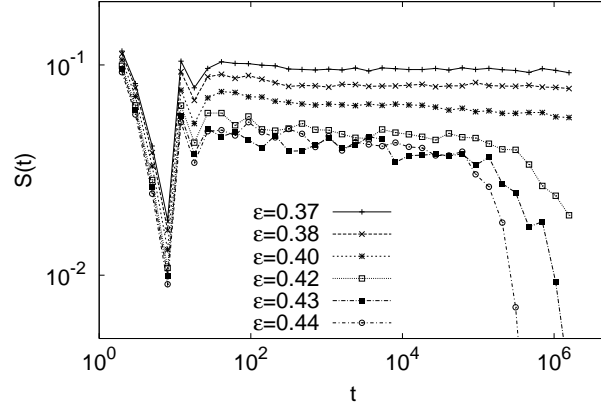


Fig. 14. Temporal evolution of the averaged order parameter $S(t)$ for the Bernoulli map with $r = 1:1$, $\epsilon = 0.8$, $L = 501$, and different coupling strength above and below ϵ_{n1} (see the labels). A average is done over 100 – 500 initial conditions, tests on shorter times and more initial conditions confirm the reliability of the statistics.

studied in [38] once the exponent is identified with 1. However, in (3) the coupling is rescaled by the factor $(\epsilon)^{-1/L}$ to avoid divergences in the limit $L \rightarrow 1$. The rescaling L^{-1} amounts to consider effective interaction on large scales of the type $1=r$ independently of ϵ . This may explain the fact that the exponents characterizing the transition of model (3) coincide with the mean-field values reported in [38] for $\epsilon = 0$. A similar rescaling was performed in Ref. [39] to show, for a chain of power-law coupled rotators, that all the equilibrium properties of the system coincide for $0 < 1$, once suitably scaled. Let us also remark that since we are dealing with a mean-field case the nature of the noise entering in the Langevin equation, which distinguishes Directed Percolation from Multiplicative Noise, is irrelevant [21,22]. This leads us to conclude that, for continuous synchronization transitions, we would not expect any differences in the measured exponents between linearly and nonlinearly driven transitions.

In examining the critical properties associated to coupled class II maps, we confronted with hard numerical difficulties related to the fact that $\epsilon_c = \epsilon_{n1}$ cannot be measured with the required precision. Moreover, due to the presence of exponentially long transients in the proximity of the nonlinear transition, simulations of model (3) with class II maps become extremely time consuming. For these reasons we were unable to find conclusive results. However, within these limitations, our analysis (performed up to $L = 501$ and up to integration times $\sim 10^6$) suggests that for class II maps (both the Bernoulli map and its continuous version (8) with $r = 1:1$ were considered) the transition may be discontinuous as suggested from the data shown in Fig. 14. In the figure the temporal evolution of the order parameter $S(t)$ averaged over many initial conditions is reported in proximity of ϵ_{n1} and no indication of critical behaviour is observable. This indicates that in class II CMLs: short range interactions give rise to DP-like continuous transitions, while power-law coupled maps

exhibit discontinuous transitions. We should mention that the introduction of long-range interactions in DP model can similarly modify the nature of the transition from continuous to discontinuous, as shown in a recent paper [27]. The authors have introduced a generalized directed percolation model, in which the activation rate of a site at the border of an inactive island of length ℓ is given by $1 + a\ell^{-\alpha}$. In particular, in Ref. [27] it has been shown that the transition is continuous for $\alpha > 1$ with exponent coinciding with DP, and discontinuous for $0 < \alpha < 1$.

4 Conclusions

In the present paper we have examined the influence of strong nonlinearities in the transverse synchronization transition of low and high dimensional chaotic systems. In particular, for two coupled maps we have shown that finite amplitude nonlinear instabilities can give rise to long transients, preceding the synchronization, even when the dynamics is transversally stable at any instant. This should be contrasted with the results found for continuous maps where long transients may happen only as a result of transient chaotic or intermittent transverse dynamics. In high dimensional systems with long range (power-law) interactions strong nonlinearities may invalidate the linear criterion to locate the critical coupling. In this case the transition occurs, due to nonlinear mechanisms, at a larger coupling value. The nonlinear transition is characterized by the emergence of transients diverging exponentially with the system size even above the linear critical coupling. The origin of this transition is closely related to the stable chaos phenomenon. The synchronization phenomena both in linearly and nonlinearly driven systems have been compared with models for long ranged contact processes. We found that, for linearly driven systems, the transition is continuous and the critical exponents are given by a mean field prediction. For nonlinearly driven systems, though the results are not conclusive, evidence of a discontinuous transition have been found.

Acknowledgements

We are grateful to W. Just, A. Politi and A. Pikovsky for useful discussions and remarks and to F. Ginelli also for a careful reading of this manuscript. Partial support from the Italian FIRB contract n. RBNE01CW 3M_001 is acknowledged.

References

- [1] D. He and L. Stone, *Proc R Soc Lond B Biol Sci.* 270 (2003) 1519.
- [2] P. N. Steinmetz, A. Roy, P. J. Fitzgerald, S. S. Hsiao, K. O. Johnson, and E. Niebur, *Nature* 404 (2000) 187.
- [3] A. Pikovsky, M. Rosenblum, and J. Kurths, *Synchronization A Universal Concept in Nonlinear Sciences*, (Cambridge University Press, 2001)
- [4] L. M. Pecora and T. L. Carroll, *Phys. Rev. Lett.* 64 (1990) 821.
- [5] S. P. Kuznetsov and A. S. Pikovsky, *Radiophys. Quantum Electron.*, 32 (1989) 49.
- [6] A. S. Pikovsky and P. Grassberger, *J. Phys. A: Math. Gen.* 24 (1991) 4587.
- [7] W. Just, *Physica D* 81 (1995) 317.
- [8] L. Baroni, R. Livi, and A. Torcini, *Phys. Rev. E* 63 (2001) 036226.
- [9] V. Ahlers and A. S. Pikovsky, *Phys. Rev. Lett.*, 88 (2002) 254101.
- [10] C. Anteneodo, S. E. de S. Pinto, A. M. Batista, and R. L. Viana, *Phys. Rev. E*, 68 (2003) 045202(R); C. Anteneodo, A. M. Batista, and R. L. Viana, *Phys. Lett. A*, 326 (2004) 227.
- [11] M. Dharmaia, V. K. Jirsa, and M. Ding, *Phys. Rev. Lett.* 92 (2004) 028101.
- [12] K. Wiesenfeld, P. Colet and S. H. Strogatz, *Phys. Rev. Lett.* 76 (1996) 404.
- [13] C. Peskin, *Mathematical Aspects of Heart Physiology* (Courant Institute of Mathematical Sciences, New York University, New York, 1975).
- [14] G. Paladin and A. Vulpiani, *J. Phys. A* 25 (1994) 4911.
- [15] A. Torcini and S. Lepri, *Phys. Rev. E*, 55 (1997) R3805.
- [16] K. Kaneko, *Physica D*, 34 (1989) 1.
- [17] I. Waller and R. Kapral, *Phys. Rev. A* 30, 2047 (1984); K. Kaneko, *Prog. Theor. Phys.* 72 (1984) 980.
- [18] V. Ahlers, *Scaling and synchronization in deterministic and stochastic nonlinear dynamical systems*, PhD Thesis (Potsdam, 2001)
- [19] F. Ginelli et al. *Phys. Rev. E* 68 (2003) 065102(R).
- [20] M. A. Munez and R. Pastor-Satorras, *Phys. Rev. Lett.* 90 (2003) 204101.
- [21] M. A. Munez, in *Advances in Condensed Matter and Statistical Mechanics*, eds. E. Konutcheva et al. (Nova Science Publishers, 2004, New York).
- [22] H. Hinrichsen, *Adv. Phys.*, 49 (2000) 815.

- [23] E. Aurell, G. Boetta, A. Crisanti, G. Paladin and A. Vulpiani, Phys. Rev. Lett. 77 (1996) 1262.
- [24] G. Boetta, M. Cencini, M. Falcioni and A. Vulpiani Phys. Rep. 356 (2002) 367.
- [25] M. Cencini and A. Torcini Phys. Rev. E 63 (2001) 056201.
- [26] W. Feller, An introduction to probability theory and its applications (Wiley, New York, 1974); H.C. Tuckwell, Introduction to theoretical neurobiology – Vol. 2 – Nonlinear and stochastic theories (Cambridge University Press, Cambridge, 1988).
- [27] F. Ginelli, H. Hinrichsen, R. Livi, D. Mukamel, and A. Politi, Phys. Rev. E 71 (2005) 026121.
- [28] A. Politi, R. Livi, G.L. Oppo and R. Kapral, Europhys. Lett. 22 (1993) 571.
- [29] A. Torcini, P. Grassberger and A. Politi, J. Phys. A 27 (1995) 4533.
- [30] A. Politi and A. Torcini, Europhys. Lett., 28 (1994) 545.
- [31] G. Paladin and A. Vulpiani, Phys. Rep. 156 (1987) 147.
- [32] H. Jeys and B.S. Jeys, in Methods of Mathematical Physics, (Cambridge, England, Cambridge University Press, 1988) pp. 470-472.
- [33] F. Ginelli, R. Livi, and A. Politi, J. Phys. A : Math. Gen. 35 (2002) 499.
- [34] A. Lipowski and M. Droz, "Synchronization and partial synchronization of linear maps", cond-mat/0312067
- [35] R. Wackerbauer and K. Showalter, Phys. Rev. Lett. 91 (2003) 174103.
- [36] A. Zumdick, M. Timme, T. Geisel, and F. Wolf, Phys. Rev. Lett. 93 (2004) 244103.
- [37] F. Ginelli, R. Livi, A. Politi, and A. Torcini Phys. Rev. E 67 (2003) 046217.
- [38] H. Hinrichsen and M. Howard, Eur. Phys. J. B 7 (1999) 635.
- [39] F. Tamarit and C. Anteneodo, Phys. Rev. Lett. 84 (2000) 208.